HOS-Based Virtual Instrument for Power Quality Assessment

Jose Mª Sierra-Fernández, Juan José González de la Rosa,
José Carlos Palomares-Salas, Agustín Agüera-Pérez, Daniel Ayora-Sedeño,
and Antonio Moreno-Muñoz

Research Gorup PAIDI-TIC-168
Escuela Politecnica Superior de Algeciras (Universidad de Cádiz) Avd. Ramón Puyon S.N.
jose.sierrafernandez@gmail.com, juanjose.delarosa@uca.es.

Abstract. This paper describes a virtual instrument for PQ assessment. Conceived to detect transients, sags and swells, the computational nucleus is based in higher-order statistics, which enhance the statistical characterization of the raw data, with the consequent improvement of the instrument's performance. This measurement application is thought to be used by the plant operator previously trained in PQ analysis. The normal operation limit is previously established on empirical expert knowledge. The instrument also allows online visualization of the statistical parameters (variance, skewness and kurtosis). The repeatability is 85% roughly. Results convey the idea of an easy transferable technology, due to its low cost and optimized computational nucleus.

Keywords: power quality, hos, virtual instrument, sag, swell, impulsive transient.

1 Introduction

Non-linear loads supporting high voltages are very common elements in power systems. Parasitic harmonics generated in this type of loads cause anomalies in the ideal power sine wave, that affect to sensitive equipments, introducing failures in its normal function and consequently provoking losses and reducing the life of many systems; e.g. induction motors [1-4]. Traditionally the analysis of deformation of power waveform was performed via FFT, wavelet transforms and other frequency decomposition system (e.g. calculating the THD).

Switching between lines during normal operation of power systems and switching loads introduce temporal voltage fluctuations (sags and swells), which affect to all interconnected systems, e.g. reductions of motor's torque, resetting electronic systems, turning off them by under voltage or destroy them by over voltage [5]. The traditional measurement procedure implemented in the monitoring equipment is based in RMS value and peak detection of the power waveform [6].

The estimators traditionally used to detect the former anomalies are based in second-order algorithms [7], which are capable of completely characterize Gaussian

M.L. Reyes et al. (Eds.): IT Revolutions 2011, LNICST 82, pp. 1–9, 2012.

signals. Nevertheless, the complexity of the electrical anomalies suggests the idea of using statistics of order 3 and more. Without any perturbation, power waveform exhibits a Gaussian behavior; non-Gaussian features provide complete information about the type of fail, generally associated with an impulsive behavior [8].

During the last ten years higher-order statistics (HOS) are being introduced in the measurement PQ algorithms as a complement with no evidence of practical implementation. We remark the advances in [8], where two types of transients are distinguished via HOS, and [9] associated to PQ and plague detection. Virtual instruments (VI) allow low-cost development and implementation;

This paper describes a VI implementing HOS for PQ targeting. The computational guts are based in second, third and fourth order estimators in the time domain, which sweep the signal under test by means of a sliding window, over which the statistics are calculated. The maximum computational power in HOS calculation is reached by adjusting the window conveniently, as described further. The paper is organized in the following way. Section 2 summarizes HOS which are implemented in the VI, described in Section 3, which gathers the instrument design users' interface and results. Finally, conclusions are drawn in Section 4.

2 Higher-Order Statistics

Higher-order cumulants are used to infer new properties about the data of non-Gaussian processes [9]. In multiple-signal processing it is very common to define the combinational relationship among the cumulants of r stochastic signals, $\{x_i\}_{i\in[1,r]}$, and their moments of order $p, p \le r$, given by using the *Leonov-Shiryaev* expression, given in Eq. (1) [10]:

$$Cum(x_1,...,x_r) = \sum (-1)^{p-1}\cdot(p-1)!\cdot E\left\{\prod_{i\in s_1} x_i\right\} E\left\{\prod_{j\in s_2} x_j\right\}\cdots E\left\{\prod_{k\in s_p} x_k\right\} \tag{1}$$

where the addition operator is extended over all the partitions, like one of the form $(s_1, s_2,..., s_p)$, with $p = 1,2,...,r$; and $(1 \le i \le p \le r)$; being s_1 a set belonging to a partition of order *p*, of the set of integers $1,...,r$.

Let $\{x(t)\}$ be an *r*th-order stationary random real-valued process. The *r*th-order cumulant is defined in Eq. (2) as the joint *r*th-order cumulant of the random variables $x(t), x(t+\tau_1),..., x(t+\tau_{r-1})$,

$$C_{r,x}(\tau_1,\tau_2,...,\tau_{r-1}) = Cum[x(t),x(t+\tau_1),...,x(t+\tau_{r-1})] \quad (2)$$

The second-, third- and fourth-order cumulants of zero-mean $x(t)$ can be expressed via Eq. (3) [11]:

$$C_{2,x}(\tau) = E\{x(t)\cdot x(t+\tau)\} \quad (3a)$$

$$C_{3,x}(\tau_1,\tau_2) = E\{x(t)\cdot x(t+\tau_1)\cdot x(t+\tau_2)\} \quad (3b)$$

$$\begin{aligned} &C_{4,x}(\tau_1,\tau_2,\tau_3) \\ &= E\{x(t)\cdot x(t+\tau_1)\cdot x(t+\tau_2)\cdot x(t+\tau_3)\} \\ &- C_{2,x}(\tau_1)C_{2,x}(\tau_2-\tau_3) \\ &- C_{2,x}(\tau_2)C_{2,x}(\tau_3-\tau_1) \\ &- C_{2,x}(\tau_3)C_{2,x}(\tau_1-\tau_2) \end{aligned} \quad (3c)$$

By putting $\tau_1=\tau_2=\tau_3=0$ in Eq. (3), we obtain Eq. (4):

$$\gamma_{2,x} = E\{x^2(t)\} = C_{2,x}(0) \quad (4a)$$

$$\gamma_{3,x} = E\{x^3(t)\} = C_{3,x}(0,0) \quad (4b)$$

$$\gamma_{4,x} = E\{x^4(t)\} - 3(\gamma_{2,x})^2 = C_{4,x}(0,0,0) \quad (4c)$$

The expressions in Eq. (4) are measurements of the variance, skewness and kurtosis of the distribution in terms of cumulants al zero lags (the central cumulants). Normalized kurtosis and skewness are defined as $\gamma_{4,x}/(\gamma_{2,x})^2$ and $\gamma_{3,x}/(\gamma_{2,x})^{3/2}$, respectively. We will use and refer to normalized quantities because they are shift and scale invariant. If $x(t)$ is symmetrically distributed, its skewness is necessarily zero (but not *vice-versa*, almost impossible situations); if $x(t)$ is Gaussian distributed, its kurtosis is necessarily zero (but not *vice versa*). In the section of results, analysis is performed using sliding cumulants, i.e. a moving window in the time domain over which to compute each cumulant (3rd and 4th-order cumulants for zero time-lag).

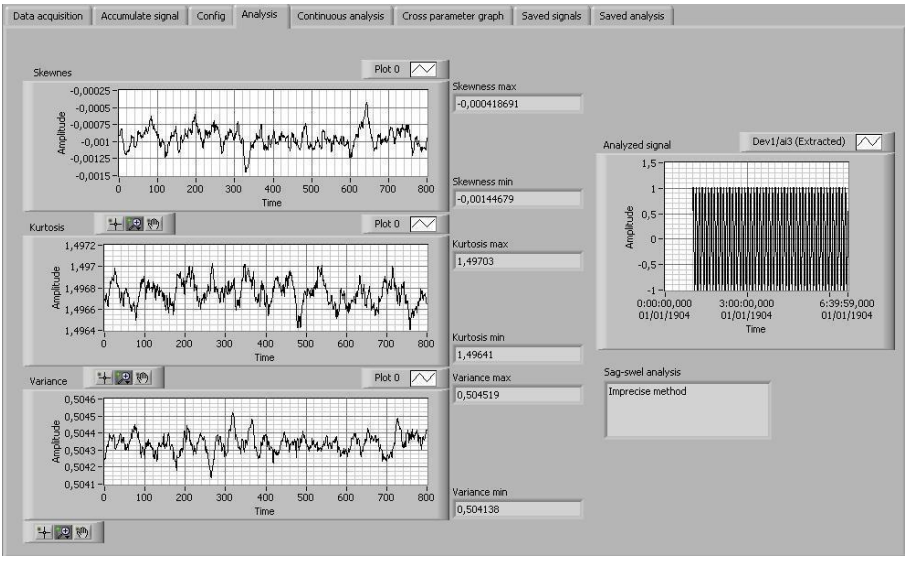

Fig. 1. "Analysis" tab

3 Instrument Design and Results

The VI analyzer has been designed in LabVIEW (ver. 8.5). It drives a PCMCIA data acquisition board (DAQ-NI-6036E). Fig. 1 shows instrument's organization, using tabs. "Analysis" is the main tab, shows the analyzed signal (last fragment of real time signal) normalized in "Analyzed signal" graph. Result of HOS analysis is plotted in the "Variance", "Skewness" and "Kurtosis" graphs. These measurement time-series constitute an example of normal operation. The horizontal axis shows the number of the window tested (iteration number within the calculation process). These peaks are evidences of the imperfections associated to the power signal, along with the noise that the acquisition board introduces. The ideal operation steady state and the observed deviation range correspond to the triplet: Variance = 0.5000 ± 0.0045, Skewness = 0.0000 ± 0.0014 and Kurtosis = 1.500 ± 0.003.

The maxima and minima values of the magnitudes are indicated next to each HOS graph. These values are compared with normal the operation limits, based on empirical experience. If these limits are trespassed, an anomaly is targeted in the signal and the VI save it for a further detailed analysis. The last indicator of this tab, "Sag-swell analysis", shows the variance calculation results. In the case shown in Fig. 1, it is displayed "Imprecise method", which means that data show a deviation less than 12 % (87 % Sag or 112 % Swell).

The rest of the VI tabs are described hereinafter. "Data acquisition" shows the configuration of the DAQ board. "Accumulate signal" shows the intermediate buffer between the acquisition and the analysis, with the objective of keeping data if occurs that the analysis is very time-consuming. The tab "Config" controls the main analysis configuration. The user must indicate a perfect signal in order to lock the normal

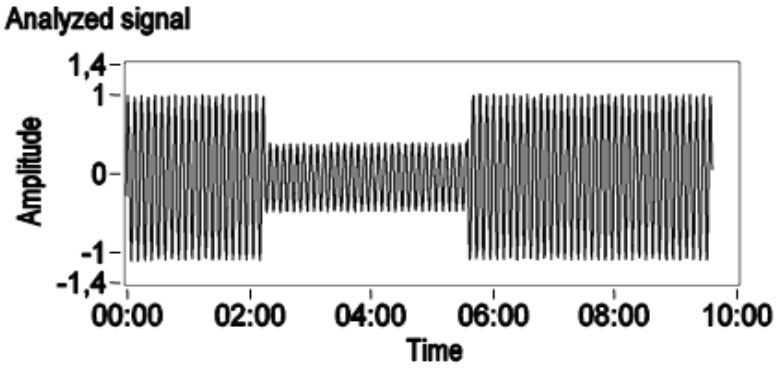

(a) Sag 40%

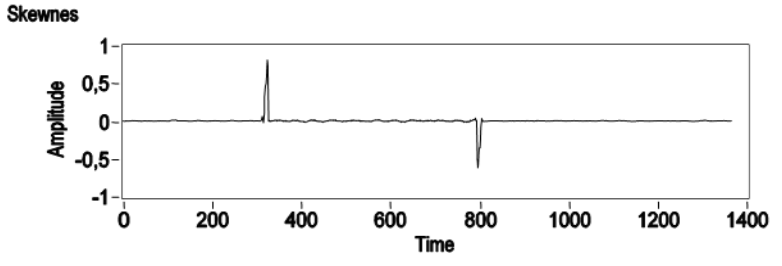

(b) Sag's skewness graph

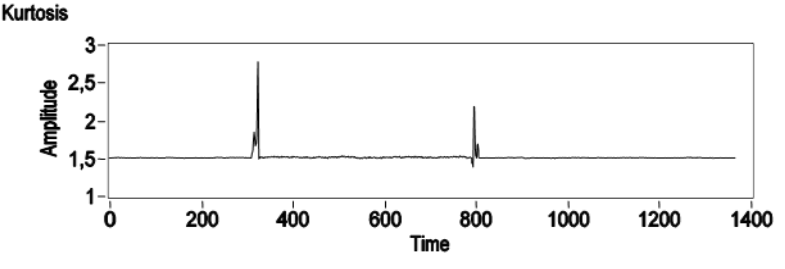

(c) Sag's kurtosis graph

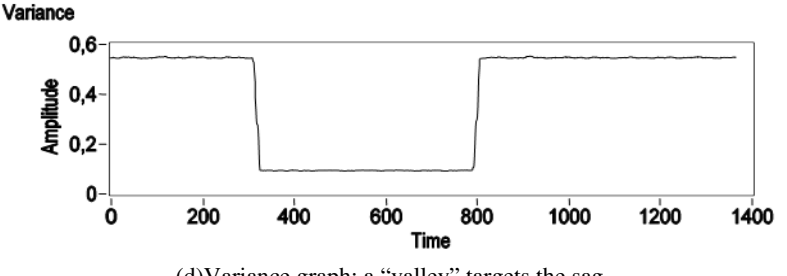

(d)Variance graph: a "valley" targets the sag

Fig. 2.

amplitude, and to modify the window's length, the "slide ratio" (window's shift data), and normal operation limits. In this situation, window's wide is 1 cycle, sliding is 25 data, and the normal operation limits for the variance range from 0.45 to 0.55, -0.02 to 0.02 for skewness and for kurtosis 1.47 to 1.53.

The tab for "Continuous analysis" gathers an historical of HOS analysis graphs. The tab for "Cross parameter graph" allows drawing a graph with some points obtained of previous simulations for different types of anomalies. The VI marks a rectangle over these defects with the associated normal operation limits, and a cross with the actual analysis values. Bi-dimensional graphs depict extremes associated to each statistical parameter, e.g. variance maximum vs. minimum. By watching the graph, the user can conclude if the signal is normal or defective.

Finally, the tabs called "Saved signals" and "Saved analysis" let the user load signals, previously saved for exceeding normal operation limits or within a historical analysis, respectively.

Due to its versatility, the VI is adaptable a wide branch of physical inputs, e.g. it has been tested too with Agilent DSO6012A Digital oscilloscope. It is even possible to join it to a bigger system with power signal data available. Besides, the system's response could be output, for example different levels of alarm, depending on the type and number of defects.

This VI has been tested with simulated data by "Agilent 6811B AC Power Source/Analyzer" instrument. These signals are different situations of Sag, Swell and impulsive transient defect types, modifying different parameters.

Fig. 2 (a) shows a normalized test signal (50 Hz – 230 V_{rms}) with a reduced zone of 50 Hz – 92 V RMS, a sag of 40 %. The normalized defect is 0.4 valued. Fig. 2 (b)-(c)-(d) show the HOS analysis graphs. The skewness sub-figure shows two impulses, around the zero steady state. These peaks are caused by the sudden change of the signal's amplitude. The sign and level of the peaks change depending on different conditions; for example the phase of the sinusoid when the sag starts or finishes changes the sign and the level. Maximum value is 0.808 and minimum -0.623, both exceeding the limits of 0.02 and -0.02, respectively.

Fig. 2 (c) shows two peaks at the same position of Fig. 2 (b), always associated to the amplitude fluctuations. They also behave differently, always over the value 1.5, and always appear in a sag-swell defect. The highest observed peak is 2.768 and the minimum is 1.377 at the starting of the second peak. Again, both exceed normal operation limits, 1.53 and 1.47 respectively.

Fig. 2 (d) is the main graph in sag-swell analysis, the variance graph. Variance is related to the amplitude's square, giving us information about amplitude evolution. The appearance is a zone of less variance during the sag, because the amplitude is a fraction of the normal operation amplitude. Maximum of this graph is 0.547, inside max normal operation limit (0.55), but minimum is 0.085, out of the min limit (0.45). For this concrete sag, all extreme values except one are out of the limits, so the instrument classifies it defective. Result of "Sag-swell analysis" is sag 40 %, which is exactly the defect present in this test, confirming the equipment calibration.

If the defect was swell (the symmetrical case of sag), the situation would be similar. The same peaks in skewness and kurtosis graphs at the defect's start and end are found. The main difference is observed in the variance graph. During the defect, the level is higher than the normal operation value, instead of the reduction associated to sag.

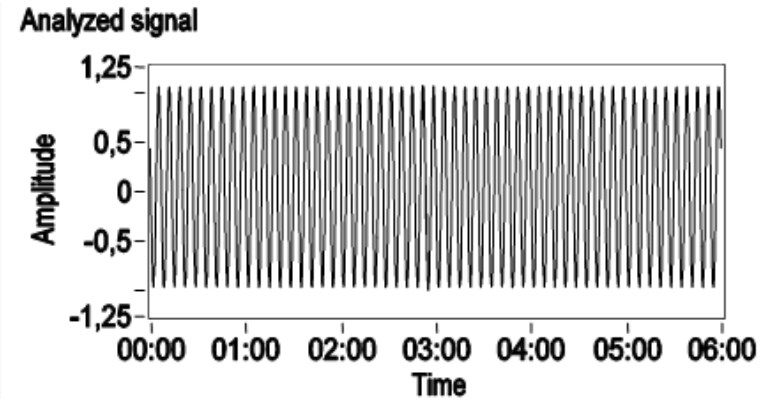

(a) Impulsive transient

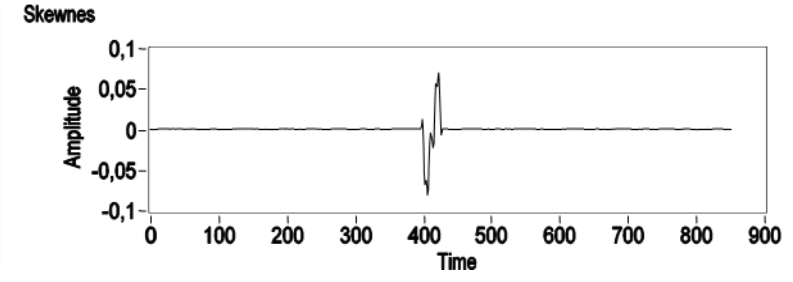

(b) Impulsive transient's skewness graph

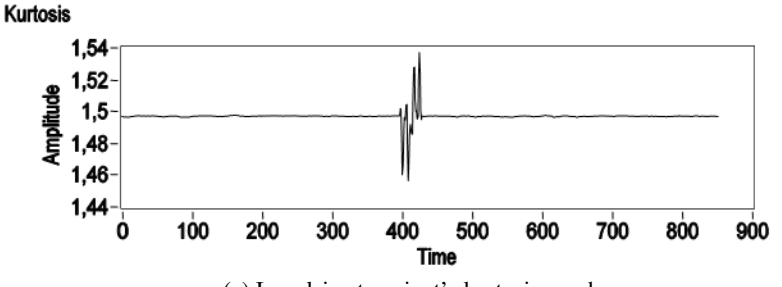

(c) Impulsive transient's kurtosis graph

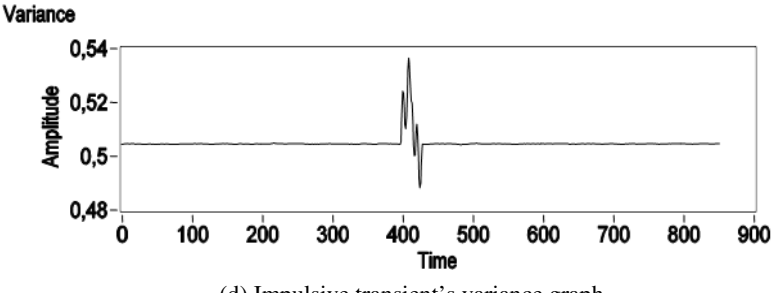

(d) Impulsive transient's variance graph

Fig. 3.

With all this, we can determine a sag defect when there is a zone with less variance (more in swell case), starting and ending with a peak in skewness and kurtosis.

At a first glance the upper sub-figure in Fig. 3, looks like a normal 50 Hz waveform, but it has a buried impulsive transient, starting in phase 170º, with maximum amplitude 30 % of normal amplitude. In this case the defect is not obvious, like the previous one.

Both peaks in Fig. 3 (b) give information about transient. Maximum value is 0.069, and minimum - 0.076, out of limits of 0.02 and -0.02.

Fig. 3 (c) is similar to Fig. 3 (b). It has peaks of similar form and exactly in the same point, created by the same transient. Skewness's peaks are similar over and less than zero, but kurtosis has a normal value of 1.5, so peaks have approximately the same extension around that value, but always positive. Maximum value is 1.536 and minimum 1.450; they are out of the limits, of 0.53 and 0.47 although maximum is very near to the limit.

Fig. 3(d) is the variance evolution. In this case, there are peaks higher to the normal value, and a little peak lower. But they are in the same place that previous peaks, exactly in the location of the defect. Maximum value is 0.537 and minimum 0.487, they are in the range of normal operation: 0.55 to 0.45.

"Sag-swell analysis" returns "Imprecise method", because conditions of Sag-swell are no present in this analysis.

In impulsive defects Skewness and Kurtosis are out of normal operation limits, but variance not. One value out of limits is enough to determine the presence of a defect, and in this case we have four.

With all this, we can determine an impulsive transient defect when there are peaks at the same place of all tree HOS graphs, and any of them are out of normal operations limits.

Test signals which have been detected are 93 sag/swell defects and 60 impulsive transient defects. This set of 153 test waveforms represents the 85% of the distorted signals which have been tested. "Sag-swell analysis" only fails in less than 12 % deviation of normal amplitude, from sag 87% to swell 112 %. In sag/swell out of that range, work perfectly. Normal operation limits has been fixed for detect all simulated defects, and ignore normal operation activity of two different signals sources and our electric power source (waveform in our plug).

4 Conclusions

This paper has shown the performance of a VI conceived to detect electrical anomalies within a range pre-defined by the user. Its computational modulus is based in HOS, giving consequently extra information beyond the Gaussian limit.

This VI has been tested with sags, swells and impulsive transients, detecting 85% of defective signals. User could change all limits, changing instrument sensibility.

Sags are targeted by the presence of a "valley" in the variance graph, as well as a peak in the skewness and kurtosis graph in the starting and finishing the "valley". Swells are detected symmetrically. Impulsive transients are detected by targeting impulses in the same position of the three graphs (skewness, variance and kurtosis).

The VI can operate online and requires an eventual presence of the panelist, with the end of checking the historical of detection hints.

Acknowledgments. The authors would like to thank the Spanish Ministry of Science and Innovation for funding the research projects TEC2009-08988 and TEC2010-19242-C03-03 (SIDER-HOSAPQ). Our unforgettable thanks to the trust we have from the Andalusian Government for funding the Research Group PAIDI-TIC-168 in Computational Instrumentation and Industrial Electronics-ICEI.

References

1. Mõlder, H., Vinnal, T., Beldjajev, V.: Harmonic Losses in Induction Motors Caused by Voltage Waveform Distortions. In: IEEE Electric Power Quality and Supply Reliability Conference (PQ), Kuressaare, Estonia, June 16-18, pp. 143–150 (2010)
2. Elmoudi, A., Lehtonen, M., Nordman, H.: Effect of harmonics on transformers loss of life. In: IEEE Electrical Insulation Conference Record of the 2006, Toronto, Ont., June 11-14, pp. 408–411 (2006)
3. Inan, A., Attar, F.: The life expectancy analysis for an electric motor due to harmonic's. In: 9th Mediterranean IEEE Electrotechnical Conference, MELECON 1998, Tel-Aviv, May 18-20, pp. 997–999 (1998)
4. Caramia, P., Carpinelli, G., Verde, P., Mazzanti, G., Cavallini, A., Montanari, G.C.: An approach to Life Estimation of Electrical Plant Components in the Presence of Harmonic Distortion. In: Proceedings of IEEE Ninth International Conference on Harmonics and Quality of Power, Orlando, FL, October 1-4, vol. 3, pp. 887–892 (2000)
5. de San Martín, J.A.Z.: Detección automática de perturbaciones en la calidad de la energía eléctrica y clasificación basada en inteligencia artificial. CURSO PEDECIBA Redes Neuronales y Memorias Distribuidas, Fac. Ciencias (2007)
6. Radil, T., Ramos, P.M., Janeiro, F.M., Serra, A.C.: PQ Monitoring System for Real-Time Detection and Classification of Disturbances in a Single-Phase Power System. In: IEEE Transactions on Instrumentation and Measurement, Braunschweig, Germany, pp. 1725–1733 (2008)
7. Wang, Z.-G., Shi, H.-S., Wang, S.: A New Harmonic Analyzer based on Wavelet and Virtual Instrument. In: IEEE International Conference on Intelligent Human-Machine Systems and Cybernetics, IHMSC 2009, Hangzhou, Zhejiang, Augusut 26-27, pp. 253–255 (2009)
8. de la Rosa, J.J.G., Moreno Muñoz, A., Gallego, A., Piotrkowski, R., Castro, E.: Higher-order characterization of power quality transients and their classification using competitive layers. Measurement 42(3), 478–484 (2009)
9. de la Rosa, J.J.G., Moreno Muñoz, A.: Higher-order cumulants and spectral kurtosis for early detection of subterranean termites. Mechanical Systems and Signal Processing 22(2), 279–294 (2008)
10. Nikias, C.L., Petropulu, A.P.: Higher-Order Spectra Analysis. A Non-Linear Signal Processing Framework. Prentice-Hall, Englewood Cliffs (1993)
11. Nikias, C.L., Mendel, J.M.: Signal processing with higher-order spectra. IEEE Signal Processing Magazine, 10–37 (1993)